



In vivo evaluation of a hyperspectral imaging system for minimally invasive surgery (HSI-MIS)

Madeleine T. Thomaßen¹ · Hannes Köhler² · Annkatrin Pfahl² · Sigmar Stelzner¹ · Matthias Mehdorn¹ · René Thieme¹ · Boris Jansen-Winkeln³ · Ines Gockel¹ · Claire Chalopin² · Yusef Moulla¹

Received: 2 October 2022 / Accepted: 6 January 2023 / Published online: 16 January 2023
© The Author(s) 2023

Abstract

Background Hyperspectral Imaging (HSI) is a reliable and safe imaging method for taking intraoperative perfusion measurements. This is the first study translating intraoperative HSI to an in vivo laparoscopic setting using a CE-certified HSI-system for minimally invasive surgery (HSI-MIS). We aim to compare it to an established HSI-system for open surgery (HSI-Open).

Methods Intraoperative HSI was done using the HSI-MIS and HSI-Open at the Region of Interest (ROI). 19 patients undergoing gastrointestinal resections were analyzed in this study. The HSI-MIS-acquired images were aligned with those from the HSI-Open, and spectra and parameter images were compared pixel-wise. We calculated the Mean Absolute Error (MAE) for Tissue Oxygen Saturation (StO₂), Near-Infrared Perfusion Index (NIR-PI), Tissue Water Index (TWI), and Organ Hemoglobin Index (OHI), as well as the Root Mean Squared Error (RMSE) over the whole spectrum. Our analysis of parameters was optimized using partial least squares (PLS) regression. Two experienced surgeons carried out an additional color-change analysis, comparing the ROI images and deciding whether they provided the same (acceptable) or different visual information (rejected).

Results HSI and subsequent image registration was possible in 19 patients. MAE results for the original calculation were StO₂_{orig.} 17.2% (± 7.7%), NIR-PI_{orig.} 16.0 (± 9.5), TWI_{orig.} 18.1 (± 7.9), OHI_{orig.} 14.4 (± 4.5). For the PLS calculation, they were StO₂_{PLS} 12.6% (± 5.2%), NIR-PI_{PLS} 10.3 (± 6.0), TWI_{PLS} 10.6 (± 5.1), and OHI_{PLS} 11.6 (± 3.0). The RMSE between both systems was 0.14 (± 0.06). In the color-change analysis; both surgeons accepted more images generated using the PLS method.

Conclusion Intraoperative HSI-MIS is a new technology and holds great potential for future applications in surgery. Parameter deviations are attributable to technical differences and can be reduced by applying improved calculation methods. This study is an important step toward the clinical implementation of HSI for minimally invasive surgery.

Keywords Hyperspectral imaging · Minimally invasive surgery · Clinical evaluation study · Gastrointestinal surgery · Laparoscopic surgery · Perfusion

Madeleine T. Thomaßen and Hannes Köhler have equally contributed to this work.

✉ Yusef Moulla
yusef.moulla@medizin.uni-leipzig.de

¹ Department of Visceral, Transplant, Thoracic and Vascular Surgery, University Hospital of Leipzig, Liebigstr. 20, 04103 Leipzig, Germany

² Innovation Center Computer Assisted Surgery (ICCAS), Faculty of Medicine, Leipzig University, Semmelweisstr. 14, 04103 Leipzig, Germany

³ Department of General, Visceral, Thoracic, and Vascular Surgery, Klinikum St. Georg, 04129 Leipzig, Germany

Abbreviations

AL	Anastomotic leakage
ASA	American society of anaesthesiologist physical status classification
BMI	Body Mass Index
CDC	Clavien-Dindo-Classification
HSI	HyperSpectral imaging
HSI-MIS	HyperSpectral imaging system for minimally invasive surgery
HSI-Open	HyperSpectral imaging system for open surgery
CG-FA	IndoCyanine green-fluorescence angiography
LED	Light-emitting diodes
LOOCV	Leave-one-patient-out cross-validation

MAE	Mean absolute error
MIS	Minimally invasive surgery
NIR-PI	Near-Infrared Perfusion Index
OHI	Organ Hemoglobin Index
PLS	Partial least squares
RGB	Red–Green–Blue
RMSE	Root mean squared error
ROI	Region of interest
SpO ₂	Oxygen saturation
StO ₂	Tissue oxygen saturation
TME	Total mesorectal excision
TWI	Tissue Water Index

Anastomotic leakage (AL) remains a feared complication in gastrointestinal surgery, potentially inducing peritonitis, severe sepsis, followed by a complex deterioration in patients' recovery. It can lead to higher morbidity, mortality, and a higher risk for permanent stoma formation when preceded by colorectal surgery [1–7]. An adequate blood supply to the anastomosis is a significant success factor in preventing AL. Surgeons usually rely on subjective evaluation of factors like bleeding from marginal vessels, pulsation of arteries, and tissue color to evaluate perfusion. Intraoperative perfusion-testing via imaging methods can reduce the occurrence of AL and improve outcomes [4]. Recent research demonstrates the applicability of IndoCyanine Green-Fluorescence Angiography (ICG-FA) for this purpose [8–12]. It can, however, trigger allergies and anaphylaxis, and is unsuitable for patients with thyroid gland diseases, renal failure, and in pregnant women.

Hyperspectral Imaging (HSI) enables spectroscopy for every image pixel. Metabolites reflect light at distinct wavelengths, e.g., oxygenated and deoxygenated hemoglobin differ in their light-absorption characteristics. The data collected can be used to take non-invasive, spatially resolved perfusion measurements [11, 13]. Previous studies reported safe and reliable results after using the HSI-system for open surgery (HSI-Open) TIVITA® Tissue (Diaspective Vision GmbH, Am Salzhaff-Pepelow, Germany), especially when determining the resection margin in colorectal surgery, or the ideal anastomotic position of the gastric conduit when constructing esophagogastric anastomoses [14–16]. It has also been successfully evaluated for detecting intestinal ischemia [13, 17, 18], wound monitoring [19–25], graft assessment in transplant surgery [26], automated cancer diagnosis [27–34], and cancer surgical margin delineation [35], as well as for the identification of anatomic structures [36–40]. So far, its use has been limited to open surgery because of the size of current cameras.

In daily routine, most gastrointestinal anastomoses are done laparoscopically or robotically. Previous limitations of intraoperative HSI application, such as large camera size

and long data acquisition times, have been overcome by the CE-certified HSI-system for minimally invasive surgery (HSI-MIS) TIVITA® Mini Endoscopy Edition (Diaspective Vision GmbH, Am Salzhaff-Pepelow, Germany) [41]. But before it can be implemented in routine surgery, it needs to be evaluated in comparison with the conventional HSI-Open to determine any differences between the systems and to see whether the HSI-Open's findings can be translated to the laparoscopic system.

The objective of this study was to compare the HSI-MIS with an established method. We aimed to detect differences between the systems and determine whether the new system is suitable for perfusion measurements in a minimally invasive setting.

Methods

The principle of hyperspectral imaging (HSI)

Hyperspectral images are defined as images where a broadband spectrum of electromagnetic waves is acquired for every single pixel. The information is visualized as a so-called hypercube with two spatial (x and y) and one spectral dimension (λ) (Fig. 1) [42]. The interaction of metabolites and molecules with light is distinct at different wavelengths, creating a unique pattern. Each pixel's spectral information reflects the substances present in that area. Each organ and tissue, therefore, creates its distinct spectral fingerprint. Computing power and advanced image-processing techniques have evolved rapidly over the last few years [43], enabling the interpretation of this immense spectral information by translating it into tissue parameters that are easy to understand. For surgical purposes, the manufacturer provides for example Oxygen Saturation (StO₂), and the Near InfraRed-Perfusion Index (NIR-PI), which enables perfusion measurements at a deeper tissue level, the Tissue Water Index (TWI) and Organ Hemoglobin Index (OHI), a proxy for erythrocyte numbers regardless of the given tissue's oxygen supply [21].

Studied population

This study was designed as an open-label, single-center, prospective, observational study to access the safety, feasibility, accuracy, and precision of the HSI-MIS. It is a stage 2a study according to the IDEAL framework [44]. Included in this study were 19 patients aged 18 years or older undergoing upper ($n=9$) or lower ($n=10$) gastrointestinal resections at the University Hospital of Leipzig between 10/09/2021 and 11/02/2022. Exclusion criteria were patients unable to consent and pregnancy.

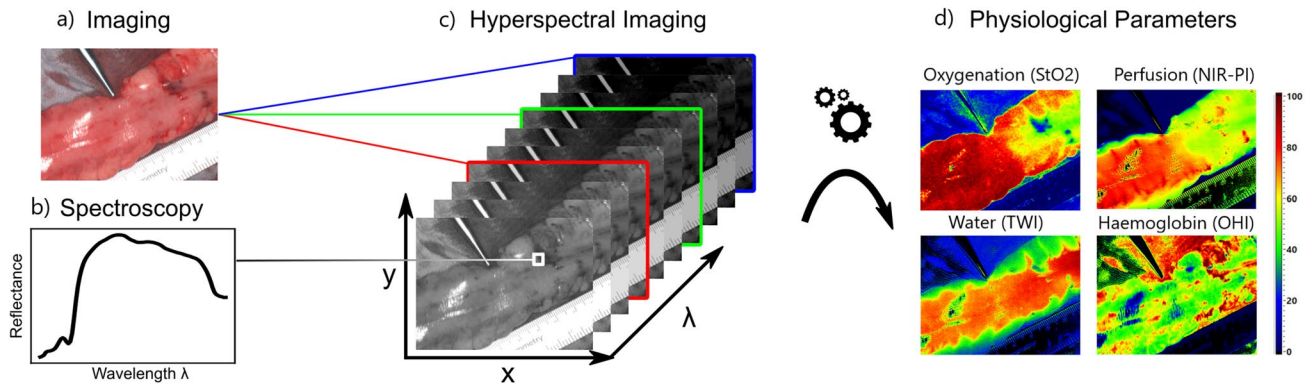


Fig. 1 The Region of Interest (ROI) is imaged, and a reconstructed color image is provided (a). Spectroscopy (b) is performed for every single pixel, creating the so-called hypercube (c). The raw spec-

tral data are used for computing the parameters (d) for Oxygenation (StO_2), Near InfraRed-Perfusion Index (NIR-PI), Tissue Water Index (TWI), and Organ Hemoglobin Index (OHI)

The institutional review board of the University of Leipzig approved this study in an amendment to ethics agreement 026/18-ek, approved initially on 31/01/2018 and registered at clinicaltrials.gov (NCT04230603) on 01/13/2020. Written informed consent was obtained from all patients.

We recorded clinical and preclinical data, such as gender and age, underlying disease, and comorbidities, specific intraoperative parameters, such as oxygen saturation (SpO_2), hemoglobin before and after the HSI measurements were taken, catecholamine application, and postoperative complications according to the Clavien-Dindo-Classification (CDC) [20].

Technology

In this study, we used these HSI-system equipments (Fig. 2): the TIVITA® Tissue camera for open surgery (HSI-Open) and TIVITA® Mini Endoscopy Edition for minimally invasive surgery (HSI-MIS) (both systems from Diaspective Vision GmbH, Am Salzhaff-Pepelow, Germany). The cameras use a push-broom scanning system. A push-broom system, also known as line scanning system, collects spectral information of one line simultaneously, and moves transversally the slit to complete the hyperspectral data cube acquisition [45]. It collects reflected light at wavelengths between 500 and 1000 nm. Within this range, 100 spectral channels are recorded, giving a spectral resolution of 5 nm. The set-up of a prototype of the HSI-MIS underwent technical evaluation by Köhler et al. [41].

Fig. 2 TIVITA® Tissue (left) and TIVITA® Mini Endoscopy Edition (right). Images provided by Diaspective Vision GmbH, Am Salzhaff-Pepelow, Germany



Table 1 Differences between the HSI-MIS and the HSI-Open

	HSI-Open	HSI-MIS
Camera size	13×9×9 cm ³	Regular laparoscopic camera case (10×5×5 cm ³)
Light source	6 halogen spots	Light-emitting diodes (LED)
Acquisition times	Appr. 10 s	7 s
Field of view (HSI)	8×6.5 cm ² at 50 cm distance	3.4×2.5 cm ² at 5 cm distance
Color Video	No	Yes

There are five main differences between the two systems (Table 1).

The camera size was reduced from 13×9×9 cm³ for the camera integrated into the HSI-Open into the size of a regular laparoscopic camera (10×5×5 cm³) in the HSI-MIS. While the HSI-Open uses six halogen spots, the HSI-MIS uses broadband Light-Emitting Diodes (LED) embedded in the computing unit positioned on a mobile cart with light transmitted via a light conductive cable. The HSI-Open's longer acquisition time (10 s) has been shortened to 7 s in the HSI-MIS. All laparoscopic measurements were taken with a 0° to 10 mm rigid laparoscope (HOPKINS® 8711 AGA, KARL STORZ SE & Co. KG, Tuttlingen, Germany) suitable for white light and near-infrared fluorescence imaging. As expected, the field of view in the laparoscopic camera is smaller than with the HSI-Open. Furthermore, the laparoscopic camera provides a color video as needed when performing minimally invasive surgery (MIS). The video runs at 55 fps and provides full-HD images with 1920×1080 pixels.

Intraoperative HSI

After having extracted the specimen and before the anastomosis, HSI was performed at the Region of Interest (ROI), which was directly proximal to the resection line (anastomosis location). All measurements were taken extraabdominally/extrathoracically. The ROI was subsequently imaged with both camera systems, and we captured at least one image per camera. The laparoscope was placed in a holding device to ensure a fixed camera position, as shown in Fig. 3. The distance between the laparoscope's tip and the ROI was kept constant at 5 cm. The room was shaded by turning off all room lights and closing the window blinds to eliminate spectral artifacts from external illumination, according to our standard protocol for intraoperative HSI measurements. Because of the unavailability of long (30 cm), and angled laparoscopes at the beginning of our study, we did not use the HSI-MIS during the whole procedure. Another reason for this was to reduce artifacts from, for example, fogging

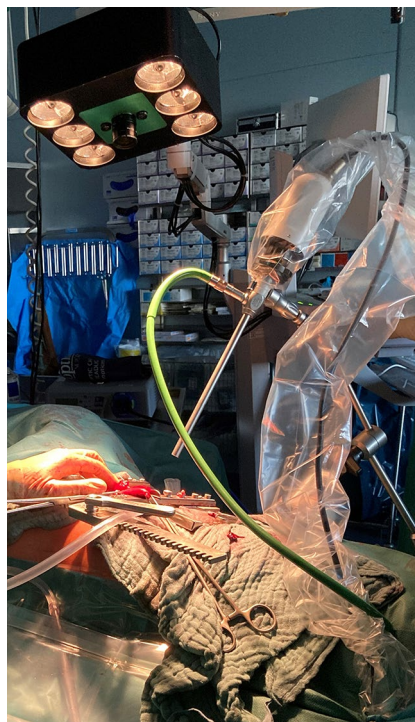


Fig. 3 The set-up shortly before taking the measurements. During data acquisition the room was darkened

or stains on the camera lens. A similar set-up for ex vivo measurements was described by Pfahl et al. [46].

Data analysis

The ROI was selected by creating a mask that excluded all image sections not showing the intestine near the resection line using the software ImageJ [47]. The images acquired with both camera systems were aligned by manually annotating 25 corresponding points and transforming the subsequent perspective (Fig. 4). Homography was obtained using OpenCV and RANSAC [48, 49] to calculate the 3×3 transformation matrix between two planes by minimizing the back-projection error. The spectra were compared per pixel by calculating the Rooted Mean Squared Error (RMSE) for the visible and near-infrared ranges. Furthermore, we calculated the Mean Absolute Error (MAE) for each tissue parameter from the absolute error between the corresponding pixels in the records. Both RMSE and MAE were averaged over all records.

The parameter calculation method used for the HSI-MIS had been developed for the HSI-Open initially and translated to the new system. To determine whether the error could be lowered by optimizing the parameter calculation method, we recalculated the parameters using partial least squares (PLS) regression [50]. PLS regression is widely used in chemometrics for multivariate spectroscopic data analysis. The

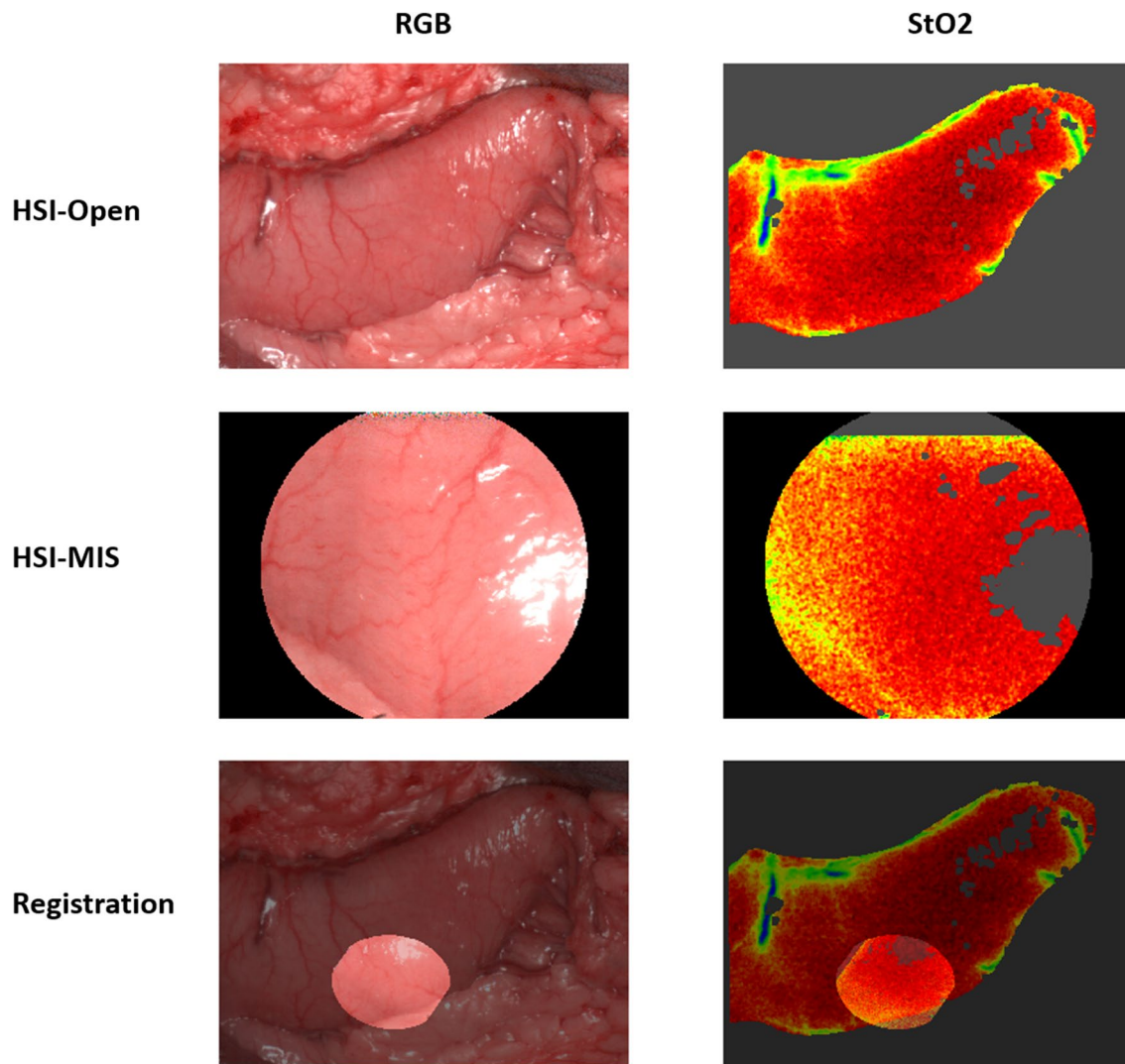


Fig. 4 Example of a completed registration. 25 points were annotated manually on both the Red–Green–Blue-image (RGB) from the HSI-MIS and the HSI-Open. An overlay was created, allowing a pixel-wise comparison of spectra

spectra acquired with the HSI-MIS were used to build the matrix of predictors, while the matrix of responses included the tissue parameters obtained from the HSI-Open. K-fold cross-validation with $k=10$ was used to determine the pre-processing and model parameters resulting in the highest determination coefficient R^2 and lowest RMSE. Nineteen PLS models were obtained during a Leave-one-patient-out cross-validation (LOOCV) and used to predict the tissue parameters from the hypercubes not used to build our model.

Surgeons often prefer to rely intraoperatively on their visual impression rather than on numbers on a screen. To create a more realistic setting reflecting intraoperative procedures, two senior abdominal surgeons with over 5 years of experience with intraoperative HSI (YM and BJW) conducted an additional analysis. The ROIs from both systems were visually compared, as were color tiles representing the

mean value for a parameter in an image. Clinically relevant color changes were those from red to yellow, green, or blue, from orange to just yellow, green, or blue, and from yellow to green or blue (Fig. 5). Red and orange represented well perfused tissue, whereas yellow, green, and blue indicated poorer perfusion. The images were rejected if the ROIs or the color tiles changed relevantly. If not, they counted as being accepted. The same analysis was carried out using the recalculated parameters from the PLS method. Before the examination, the images were randomized, and we conducted a single-blinded analysis to ensure that the surgeons had not preferred either the original or the PLS calculation method. The images were randomly placed in folders and the original and PLS images were given the same name. The average number of images rejected and accepted per surgeon was calculated, and the average MAE of the rejected

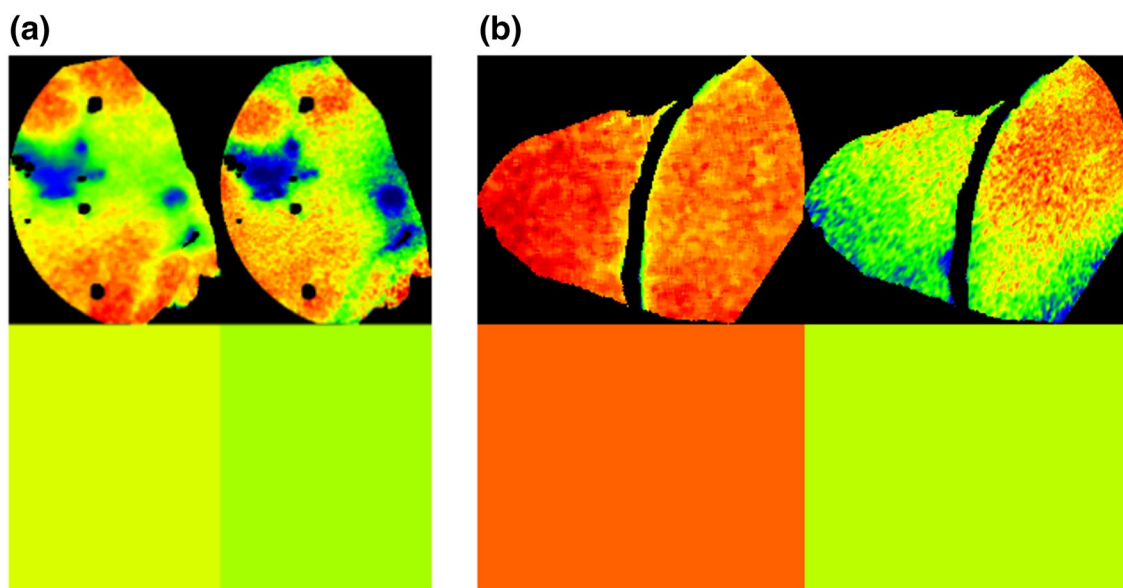


Fig. 5 StO₂ in matching areas (ROI, upper image) and color tiles visualizing the mean StO₂ (lower, square image) for the HSI-Open and the HSI-MIS. In the case of **a**, the images were accepted as showing

and accepted images was compared. Cohen's κ coefficient was calculated to measure the level of interobserver agreement [51]

Results

The study flow chart in Fig. 6 visualizes our set-up and patient selection. Twenty-three patients were eligible for the study. Four were excluded because the surgical strategy had to be changed before the measurements were performed ($N=1$), and the HSI-MIS image quality was insufficient or out of focus ($N=3$). Included patients underwent esophagectomy ($N=9$), proctocolectomy ($N=1$), hemicolectomy ($N=7$) and low anterior rectal resection with total mesorectal excision (TME) ($N=2$). Seventeen patients underwent oncological resections, one underwent hemicolectomy for abscess removal and another one proctocolectomy for ulcerative colitis treatment. The average age of patients was $63.1 (\pm 14.4)$ years, with an average BMI of $28.2 (\pm 6.1)$ kg/m². Selected patient characteristics are listed in Table 2.

HSI was safe and feasible in all 19 patients. The intraoperative procedures and surgical workflow went smoothly in all patients, as the HSI measurements (by conventional and miniature systems) took only few seconds to acquire visual information and process data. Minor incidents included connectivity problems requiring the restart of the HSI-MIS, and surgery prolonged by about one minute per restart. As the images had revealed many movement artifacts during the

the same visual expression, in the case of **b** the image was rejected for making different visual impressions (Color figure online)

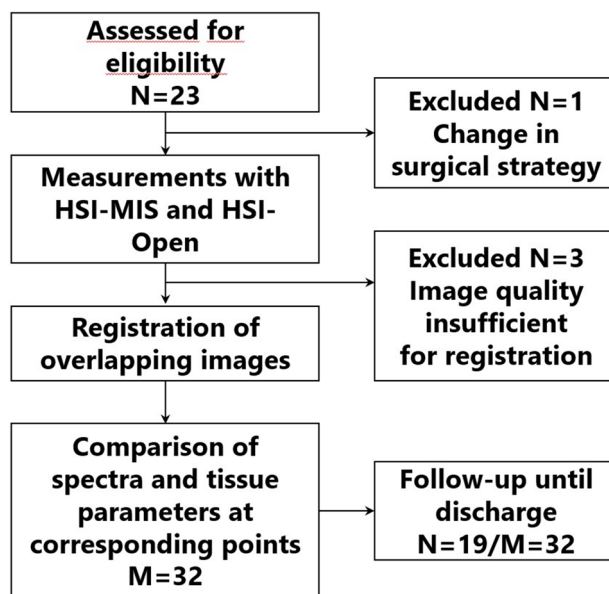


Fig. 6 The study's flow chart visualizes patient selection and trial set-up, with N =number of patients and M =number of images registered successfully

preliminary measurements, we later had to use a laparoscopic holding device.

Thirty-two images (M) were collected and registered to compare spectra and tissue parameters at corresponding points. An average of $20,146 (\pm 7,996)$ spectra were obtained per patient.

Table 2 Selected patient characteristics

Patient Characteristics (Total N=19)	N
Female	6
Male	13
BMI > 30 kg/m ²	6
Arteriosclerosis	5
Arterial Hypertension	16
Neoadjuvant Chemotherapy	13
ASA I	1
ASA II	9
ASA III	9

MAE values (Fig. 7) between the HSI parameters provided by the HSI-Open and HSI-MIS system and using the manufacturer's (original) and the PLS method were $StO_2_{orig.}$ 17.2% ($\pm 7.7\%$), StO_2_{PLS} 12.6% ($\pm 5.2\%$), $NIR-PI_{orig.}$ 16.0 (± 9.5), $NIR-PI_{PLS}$ 10.3 (± 6.0), $TWI_{orig.}$ 18.1 (± 7.9), TWI_{PLS} 10.6 (± 5.1), $OHI_{orig.}$ 14.4 (± 4.5), and OHI_{PLS} 11.6 (± 3.0).

These were remarkably reduced when using the PLS method, with improvements ranging from 19.2 to 42.3% when compared to the original calculation (Fig. 7). The TWI revealed the largest improvement for and the OHI the smallest.

The mean RMSE value between spectra was 0.14 (± 0.06), with a mean RMSE of 0.13 (± 0.06) in the visual range (500–750 nm) and a mean RMSE of 0.16 (± 0.06) in the near-infrared (750–1000 nm) range.

Concerning our color-change analysis results, the PLS method proved to raise the average number of images accepted for all parameters (Fig. 8). Improvement was greatest for the StO_2 and OHI, and smallest for the NIR-PI. We

noted a high level of interobserver variability (Table 3) with Cohen's coefficient $\kappa=0.25$. 87.5% of those images rejected by surgeon one were also dismissed by surgeon two. Surgeon two rejected many other images: while surgeon one rejected 48 out of 256 images, surgeon two rejected 135 out of 256 images. However, both surgeons accepted more images when they had been calculated via the PLS method. For the original method, the accepted images of all parameters had an average MAE of 11.0 (± 4.6) units, whereas the average MAE of all rejected images was 19.5 (± 7.3) units. For the PLS method, it was 9.3 (± 3.2) versus 14.0 (± 5.9) units.

Discussion

Our study aims to enable the first translation of HSI for MIS within an in vivo setting. Its use proved to be safe and feasible in all patients. The original calculation's MAE amounted to between almost 15 units or slightly above that. The error was greatly reduced to around 10 units using a different calculation mode (the PLS method). This finding was supported by the (blinded) visual analysis of the HSI parameter images by two experienced surgeons. While only 15.5 out of 32 StO_2 images were accepted on average when computed using the original method, 24 were accepted after optimization with the PLS model. The OHI, TWI, and NIR-PI revealed similar improvements. Surgeon two rejected almost all those images rejected by surgeon one and many additional images. However, both surgeons rejected fewer images that had been calculated via the PLS method.

This study is the first to evaluate in vivo an HSI camera designed for routine use in MIS. It is an essential step toward the clinical implementation of laparoscopic hyperspectral imaging. We were able to compare a vast number of spectra

Fig. 7 Mean absolute error (MAE) with 95% confidence intervals for the original (= manufacturer's, orig.) calculation and the calculation using partial least squares (PLS). The confidence intervals were $StO_2_{orig.}$ (14.6%, 19.9%), StO_2_{PLS} (10.8%, 14.4%), $NIR-PI_{orig.}$ (12.7, 19.3), $NIR-PI_{PLS}$ (8.2, 12.3), $TWI_{orig.}$ (15.4, 20.9), TWI_{PLS} (8.8, 12.3), $OHI_{orig.}$ (12.8, 16.0), OHI_{PLS} (10.5, 12.6)

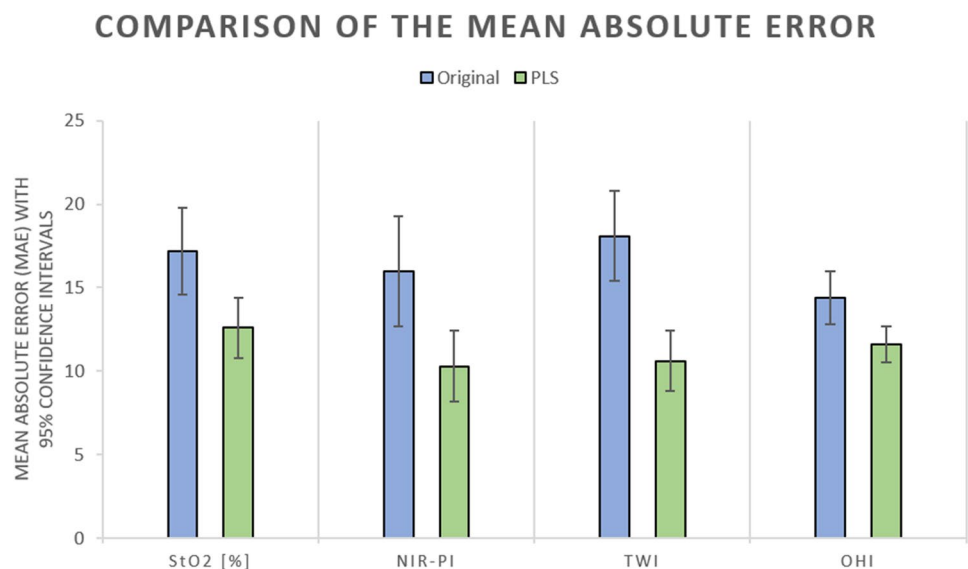


Fig. 8 Color change (visual) comparison of parameter images at the ROI and color tiles visualizing the mean value of a parameter at the ROI via the original (= manufacturer's) calculation vs. the optimized calculation using the PLS method for Oxygen Saturation (StO₂), Near-Infrared Perfusion Index (NIR-PI), Tissue Water Index (TWI) and Organ Hemoglobin Index (OHI)

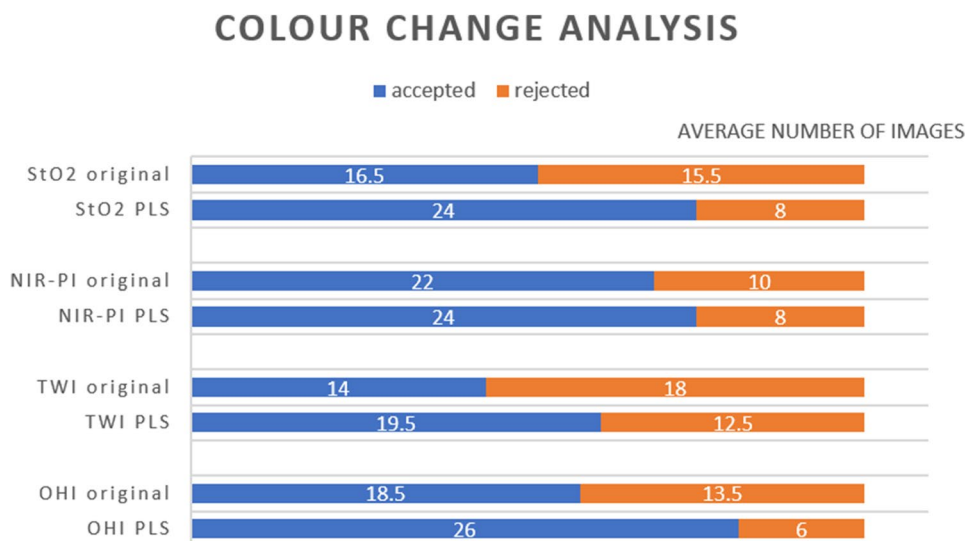


Table 3 Number of images accepted/rejected per surgeon. Both surgeons accepted the same 115 and rejected the same 42 images

		Surgeon 2		Total
		Accepted	Rejected	
Surgeon 1	Accepted	115	93	208
	Rejected	6	42	48
	Total	121	135	256

Surgeon 1 accepted additional 93 images, that Surgeon 2 rejected, whereas Surgeon 2 accepted 6 images, that Surgeon 1 rejected

per patient. Our findings create the framework for future, more extensive studies using HSI-MIS and approximating the expected error. Our investigation enabled the gathering of information about handling this system, and revealed minor technical limitations, such as connectivity issues, which were reported and fixed later by the company. We also managed to define means of improvement, namely by optimizing the calculation method.

Preliminary testing prior to this study revealed parameter images with many movement artifacts when the HSI-MIS is manually held. These affected only the spatial information, while the spectral information remained correct. To obtain images suited for matching, we placed the laparoscope in a holding device. Surgeons need a similar device to obtain equally accurate images. For clinical surgery, where no matching is required, a surgeon can obtain well interpretable hand-held images, if the laparoscope is held still. We recommend that future cameras are outfitted with an image-stabilization function.

Limitations of this pilot study are the limited number of patients included and the setting. Although performed on in vivo tissues, our study did not precisely mimic HSI's intraoperative laparoscopic application, since the

measurements were taken extracorporeally (extraabdominally/extrathoracically) during resections. Currently, both HSI and ICG-FA are established methods for measuring the perfusion of abdominal organs intraoperatively. Although ICG-FA is used more regularly in many clinics, we did not use it as a reference imaging method, since the two modalities measure different parameters and use different technology. Quantitative ICG-FA analyses the inflow-curve of an exogenous dye, whereas HSI measures physiological tissue parameters, such as StO₂, TWI, OHI, and NIR-PI. Therefore, the comparison to a camera that uses the same type of technology and the same parameters seemed better suited for this first in vivo study. In order to compare it to the established HSI-system and enable a pixel-wise comparison of spectra, the same region had to be imaged without moving the tissue between measurements. Only tissue retrieved extracorporeally was measured, as we could not obtain intracorporal images with the HSI-Open. Because only a short laparoscope (20 cm) was available when the first images were acquired and to reduce artifacts, we were not able to perform the whole procedure using the HSI-MIS. Although HSI has been assessed in different surgical disciplines, its suitability for laparoscopic surgery remains limited, and no system has been adopted for routine clinical use. Prototypes of the now CE-certified HSI-MIS were recently evaluated ex vivo [41, 46], revealing an MAE of about 10 units, and higher for each parameter. Our findings for the original calculation of the physiological parameters were slightly higher than the MAE reported by Pfahl et al. [46], while the MAE matched previous results when applying the PLS method. Therefore, part of the error is inherent to the system hardware, and part is due to how the parameters are calculated. Differences in build-up comprise lenses, sensors, and light sources. The error resulting from calculating the parameters could be reduced, leading to a better correlation between the

two systems. The influence of additional factors, such as distance between the ROI and laparoscope, was not investigated in this study. This must be done in future studies. Concerning our color-change analysis, notice that it was a subjective one carried out by two surgeons only with only a fair level of agreement. The scale was chosen by the surgeons based on their clinical expertise, thereby not externally validated. We blinded the surgeons to increase internal validity. We decided on this to simulate a setting more closely resembling actual, live surgery; our findings should be considered as a qualitative add-on analysis to objective analyses determining the MAE and RMSE.

This study's results lay the foundation for future in vivo studies using laparoscopic HSI under real operation conditions, showing that it can be safely and efficiently implemented in MIS. Larger, multi-centered studies are needed to verify the findings of this first in vivo analysis. Another goal is to perform a whole procedure with the HSI-MIS. Future studies could also comprise perfusion measurements of in situ anastomoses and comparisons between HSI-MIS and other established methods for assessing perfusion, such as quantitative ICG-FA. Other possible applications include detecting at-risk structures and differentiating cancerous from non-cancerous tissue.

Intraoperative HSI for minimally invasive procedures is a new and promising technology holding great potential for future applications in surgery.

Funding Open Access funding enabled and organized by Projekt DEAL. This research did not receive any specific grant from funding agencies in the public, commercial, or not-for-profit sectors. KARL STORZ SE & Co. KG (Tuttlingen, Germany) and Diaspective Vision GmbH (Am Salzhaff-Pepelow, Germany) provided the equipment for the measurements.

Declarations

Disclosures KARL STORZ SE & Co. KG (Tuttlingen, Germany) and Diaspective Vision GmbH (Am Salzhaff-Pepelow, Germany) provided the equipment for the measurements. Hannes Köhler is a former employee of Diaspective Vision GmbH (until 07/2020). Madeleine T. Thomaßen, Annkatrin Pfahl, Sigmar Stelzner, Matthias Mehdorn, René Thieme, Boris Jansen-Winkeln, Ines Gockel, Claire Chalopin, and Yusef Moulla have no conflicts of interest to disclose.

Open Access This article is licensed under a Creative Commons Attribution 4.0 International License, which permits use, sharing, adaptation, distribution and reproduction in any medium or format, as long as you give appropriate credit to the original author(s) and the source, provide a link to the Creative Commons licence, and indicate if changes were made. The images or other third party material in this article are included in the article's Creative Commons licence, unless indicated otherwise in a credit line to the material. If material is not included in the article's Creative Commons licence and your intended use is not permitted by statutory regulation or exceeds the permitted use, you will need to obtain permission directly from the copyright holder. To view a copy of this licence, visit <http://creativecommons.org/licenses/by/4.0/>.

References

1. Sammour T, Hayes IP, Jones IT et al (2018) Impact of anastomotic leak on recurrence and survival after colorectal cancer surgery: a BioGrid Australia analysis. *ANZ J Surg* 88:E6–E10. <https://doi.org/10.1111/ans.13648>
2. Floodeen H, Hallböök O, Rutegård J et al (2013) Early and late symptomatic anastomotic leakage following low anterior resection of the rectum for cancer: are they different entities? *Colorectal Dis* 15:334–340. <https://doi.org/10.1111/j.1463-1318.2012.03195.x>
3. Li Y-W, Lian P, Huang B et al (2017) Very early colorectal anastomotic leakage within 5 post-operative days: a more severe subtype needs relaparotomy. *Sci Rep* 7:39936. <https://doi.org/10.1038/srep39936>
4. Kryzauskas M, Bausys A, Jakubauskas M et al (2020) Intraoperative testing of colorectal anastomosis and the incidence of anastomotic leak: a meta-analysis. *Medicine (Baltimore)* 99:e23135. <https://doi.org/10.1097/MD.00000000000023135>
5. Dauser B, Herbst F (2014) Diagnosis, management and outcome of early anastomotic leakage following colorectal anastomosis using a compression device: is it different? *Colorectal Dis* 16:O435–O439. <https://doi.org/10.1111/codi.12742>
6. Mariette C, Markar SR, Dabakuyo-Yonli TS et al (2019) Hybrid minimally invasive esophagectomy for esophageal cancer. *N Engl J Med* 380:152–162. <https://doi.org/10.1056/NEJMoa1805101>
7. Zuzak KJ, Naik SC, Alexandrakis G et al (2007) Characterization of a near-infrared laparoscopic hyperspectral imaging system for minimally invasive surgery. *Anal Chem* 79:4709–4715. <https://doi.org/10.1021/ac070367n>
8. Boni L, David G, Dionigi G et al (2016) Indocyanine green-enhanced fluorescence to assess bowel perfusion during laparoscopic colorectal resection. *Surg Endosc* 30:2736–2742. <https://doi.org/10.1007/s00464-015-4540-z>
9. James DRC, Ris F, Yeung TM et al (2015) Fluorescence angiography in laparoscopic low rectal and anorectal anastomoses with pinpoint perfusion imaging—a critical appraisal with specific focus on leak risk reduction. *Colorectal Dis* 17(Suppl 3):16–21. <https://doi.org/10.1111/codi.13033>
10. Foppa C, Denoya PI, Tarta C et al (2014) Indocyanine green fluorescent dye during bowel surgery: are the blood supply “guessing days” over? *Tech Coloproctol* 18:753–758. <https://doi.org/10.1007/s10151-014-1130-3>
11. Clancy NT, Arya S, Stoyanov D et al (2015) Intraoperative measurement of bowel oxygen saturation using a multispectral imaging laparoscope. *Biomed Opt Express* 6:4179–4190. <https://doi.org/10.1364/BOE.6.004179>
12. Son GM, Kwon MS, Kim Y et al (2019) Quantitative analysis of colon perfusion pattern using indocyanine green (ICG) angiography in laparoscopic colorectal surgery. *Surg Endosc* 33:1640–1649. <https://doi.org/10.1007/s00464-018-6439-y>
13. Akbari H, Kosugi Y, Kojima K et al (2010) Detection and analysis of the intestinal ischemia using visible and invisible hyperspectral imaging. *IEEE Trans Biomed Eng* 57:2011–2017. <https://doi.org/10.1109/TBME.2010.2049110>
14. Jansen-Winkeln B, Holfert N, Köhler H et al (2019) Determination of the transection margin during colorectal resection with hyperspectral imaging (HSI). *Int J Colorectal Dis* 34:731–739. <https://doi.org/10.1007/s00384-019-03250-0>
15. Jansen-Winkeln B, Dvorak M, Köhler H et al (2022) Border line definition using hyperspectral imaging in colorectal resections. *Cancers (Basel)*. <https://doi.org/10.3390/cancers14051188>
16. Köhler H, Jansen-Winkeln B, Maktabi M et al (2019) Evaluation of hyperspectral imaging (HSI) for the measurement of ischemic conditioning effects of the gastric conduit during

- esophagectomy. *Surg Endosc* 33:3775–3782. <https://doi.org/10.1007/s00464-019-06675-4>
17. Mehdorn M, Köhler H, Rabe SM et al (2020) Hyperspectral imaging (HSI) in acute mesenteric ischemia to detect intestinal perfusion deficits. *J Surg Res* 254:7–15. <https://doi.org/10.1016/j.jss.2020.04.001>
 18. Barberio M, Felli E, Seyller E et al (2020) Quantitative fluorescence angiography versus hyperspectral imaging to assess bowel ischemia: a comparative study in enhanced reality. *Surgery* 168:178–184. <https://doi.org/10.1016/j.surg.2020.02.008>
 19. Yudovsky D, Nouvong A, Pilon L (2010) Hyperspectral imaging in diabetic foot wound care. *J Diabetes Sci Technol* 4:1099–1113. <https://doi.org/10.1177/193229681000400508>
 20. Yudovsky D, Nouvong A, Schomacker K et al (2011) Monitoring temporal development and healing of diabetic foot ulceration using hyperspectral imaging. *J Biophotonics* 4:565–576. <https://doi.org/10.1002/jbio.201000117>
 21. Holmer A, Marotz J, Wahl P et al (2018) Hyperspectral imaging in perfusion and wound diagnostics—methods and algorithms for the determination of tissue parameters. *Biomed Tech (Berl)* 63:547–556. <https://doi.org/10.1515/bmt-2017-0155>
 22. Khaodhiar L, Dinh T, Schomacker KT et al (2007) The use of medical hyperspectral technology to evaluate microcirculatory changes in diabetic foot ulcers and to predict clinical outcomes. *Diabetes Care* 30:903–910. <https://doi.org/10.2337/dc06-2209>
 23. Denstedt M (2013) Hyperspectral imaging as adiaagnostic tool for chronic skin ulcers. *Photonic Therapeutics Diagn* 8565:71–84
 24. Calin MA, Coman T, Parasca SV et al (2015) Hyperspectral imaging-based wound analysis using mixture-tuned matched filtering classification method. *J Biomed Opt* 20:46004. <https://doi.org/10.1117/1.JBO.20.4.046004>
 25. Saiko G, Lombardi P, Au Y et al (2020) Hyperspectral imaging in wound care: a systematic review. *Int Wound J* 17:1840–1856. <https://doi.org/10.1111/iwj.13474>
 26. Sucher R, Wagner T, Köhler H et al (2020) Hyperspectral imaging (HSI) of human kidney allografts. *Ann Surg.* <https://doi.org/10.1097/SLA.0000000000004429>
 27. Beaulieu RJ, Goldstein SD, Singh J et al (2018) Automated diagnosis of colon cancer using hyperspectral sensing. *Int J Med Robot* 14:e1897. <https://doi.org/10.1002/rcs.1897>
 28. Halicek M, Fabelo H, Ortega S et al (2019) In-vivo and ex-vivo tissue analysis through hyperspectral imaging techniques: revealing the invisible features of cancer. *Cancers (Basel)*. <https://doi.org/10.3390/cancers11060756>
 29. Kiyotoki S, Nishikawa J, Okamoto T et al (2013) New method for detection of gastric cancer by hyperspectral imaging: a pilot study. *J Biomed Opt* 18:26010. <https://doi.org/10.1117/1.JBO.18.2.026010>
 30. Kumashiro R, Konishi K, Chiba T et al (2016) Integrated endoscopic system based on optical imaging and hyperspectral data analysis for colorectal cancer detection. *Anticancer Res* 36:3925–3932
 31. Leavesley SJ, Walters M, Lopez C et al (2016) Hyperspectral imaging fluorescence excitation scanning for colon cancer detection. *J Biomed Opt* 21:104003. <https://doi.org/10.1117/1.JBO.21.10.104003>
 32. Liu N, Guo Y, Jiang H et al (2020) Gastric cancer diagnosis using hyperspectral imaging with principal component analysis and spectral angle mapper. *J Biomed Opt* 25:1–9. <https://doi.org/10.1117/1.JBO.25.6.066005>
 33. Martin ME, Wabuyele MB, Chen K et al (2006) Development of an advanced hyperspectral imaging (HSI) system with applications for cancer detection. *Ann Biomed Eng* 34:1061–1068. <https://doi.org/10.1007/s10439-006-9121-9>
 34. Regeling B, Laffers W, Gerstner AOH et al (2016) Development of an image pre-processor for operational hyperspectral laryngeal cancer detection. *J Biophotonics* 9:235–245. <https://doi.org/10.1002/jbio.201500151>
 35. Lu G, Halig L, Wang D et al (2014) Hyperspectral imaging for cancer surgical margin delineation: registration of hyperspectral and histological images. *Proc SPIE Int Soc Opt Eng* 9036:90360S. <https://doi.org/10.1117/12.2043805>
 36. Seidlitz S, Sellner J, Odenthal J et al (2022) Robust deep learning-based semantic organ segmentation in hyperspectral images. *Med Image Anal* 80:102488. <https://doi.org/10.1016/j.media.2022.102488>
 37. Akbari H, Kosugi Y, Kojima K et al (2009) Blood vessel detection and artery-vein differentiation using hyperspectral imaging. *Annu Int Conf IEEE Eng Med Biol Soc* 2009:1461–1464. <https://doi.org/10.1109/IEMBS.2009.5332920>
 38. Maktabi M, Köhler H, Ivanova M et al (2020) Classification of hyperspectral endocrine tissue images using support vector machines. *Int J Med Robot* 16:1–10. <https://doi.org/10.1002/rcs.2121>
 39. Cervantes-Sanchez F, Maktabi M, Köhler H et al (2021) Automatic tissue segmentation of hyperspectral images in liver and head neck surgeries using machine learning. *Artif Intell Surg.* <https://doi.org/10.20517/ais.2021.05>
 40. Studier-Fischer A, Seidlitz S, Sellner J et al (2022) Spectral organ fingerprints with machine learning-based intraoperative tissue classification with hyperspectral imaging in a porcine model. *Sci Rep* 12:11028. <https://doi.org/10.1038/s41598-022-15040-w>
 41. Köhler H, Kulcke A, Maktabi M et al (2020) Laparoscopic system for simultaneous high-resolution video and rapid hyperspectral imaging in the visible and near-infrared spectral range. *J Biomed Opt.* <https://doi.org/10.1117/1.JBO.25.8.086004>
 42. Amigo JM (2019) Hyperspectral and multispectral imaging: setting the scene. *Hyperspectral imaging.* Elsevier, Amsterdam, pp 3–16
 43. Clancy NT, Jones G, Maier-Hein L et al (2020) Surgical spectral imaging. *Med Image Anal* 63:101699. <https://doi.org/10.1016/j.media.2020.101699>
 44. McCulloch P, Cook JA, Altman DG et al (2013) IDEAL framework for surgical innovation 1: the idea and development stages. *BMJ.* <https://doi.org/10.1136/bmj.f3012>
 45. Amigo JM, Grassi S (2019) Configuration of hyperspectral and multispectral imaging systems. *Hyperspectral imaging.* Elsevier, Amsterdam, pp 17–34
 46. Pfahl A, Köhler H, Thomaßen MT et al (2022) Video: clinical evaluation of a laparoscopic hyperspectral imaging system. *Surg Endosc.* <https://doi.org/10.1007/s00464-022-09282-y>
 47. Schneider CA, Rasband WS, Eliceiri KW (2012) NIH image to imagej: 25 years of image analysis. *Nat Methods* 9:671–675. <https://doi.org/10.1038/nmeth.2089>
 48. Fischler MA, Bolles RC (1981) Random sample consensus. *Commun ACM* 24:381–395. <https://doi.org/10.1145/358669.358692>
 49. Bradski GR, Kaehler A (2011) *Learning OpenCV: Computer vision with the OpenCV library*, 1. ed., [Nachdr.]. Software that sees. O'Reilly, Beijing
 50. Geladi P, Kowalski BR (1986) Partial least-squares regression: a tutorial. *Anal Chim Acta* 185:1–17. [https://doi.org/10.1016/0003-2670\(86\)80028-9](https://doi.org/10.1016/0003-2670(86)80028-9)
 51. McHugh ML (2012) Interrater reliability: the kappa statistic. *Biochem Med (Zagreb)* 22:276–282

Publisher's Note Springer Nature remains neutral with regard to jurisdictional claims in published maps and institutional affiliations.